Quantifying moment redistribution in FRP-strengthened RC beams

Abbas Tajaddini[1, 6], Tim Ibell[2], Antony Darby[3], Mark Evernden[4], and Pedro Silva[5]

[1] Research assistant, Department of Architecture and Civil Engineering, University of Bath, UK, BA2 7AY
[2] Professor, Department of Architecture and Civil Engineering, University of Bath, UK
[3] Reader, Department of Architecture and Civil Engineering, University of Bath, UK
[4] Senior lecturer, Department of Architecture and Civil Engineering, University of Bath, UK
[5] Professor, School of Engineering and Applied Science, the George Washington University, Washington, USA
[6] Corresponding E-mail address: A.Tajaddini@bath.edu; Tel: +44 1225 385206

Date submitted for the revised draft: 28/03/2016; Word count: 4771; Number of figures: 9; Number of tables: 2

ABSTRACT

Consideration of moment redistribution (MR) in the design of continuous reinforced concrete (RC) beams results in an efficient and economical design. Adding fibre-reinforced polymer (FRP) materials to RC structures to enhance flexural capacity leads to a reduction in ductility such that design standards severely limit the exploitation of MR in the design of FRP strengthening systems. This has forced engineers to use elastic analyses for the strengthening design which leads to waste of FRP materials under many circumstances. To overcome this, complicated or empirical solutions have been applied to solve the problem of MR in FRP-strengthened RC members, with limited success. This paper presents a novel theoretical strategy for quantifying and tracking MR in such members by employing basic structural mechanics without any need for estimating rotation capacity or ductility. Fully non-linear flexural behaviour of continuous FRP-strengthened members can be predicted, and any geometry, loading arrangement and strengthening technique or configuration can be considered. The numerical model is validated against existing experimental data from the literature. Good agreement is shown between the experimental and numerical data, with the significance of this work being that, potentially, for the first time MR could credibly and confidently be incorporated into design guides for FRP strengthening of RC structures.

1. INTRODUCTION

There are various reasons why existing reinforced concrete (RC) structures may require strengthening or retrofitting. This may be because of a need for greater strength, durability or even ductility. Adding fibre reinforced polymer (FRP) materials to RC structures has been recognised as an effective technique to enhance the strength and durability of such structures (Hollaway and Leeming, 1999; Teng *et al.*, 2001). However, research has demonstrated that FRP strengthening of flexural members reduces their original ductility prior to FRP debonding (El-Refaie *et al.*, 2003; Casadei *et al.*, 2003; Oehlers and Seracino, 2004; Oehlers *et al.*, 2007). The elastic nature of the FRP generally leads to a more brittle failure of FRP-strengthened RC members.

Ductility is an intrinsic characteristic in many materials which allows them to deform plastically before failure. Beeby (1997) discussed that one of the major advantages of ductility is that bending moment (BM) can be redistributed automatically in a ductile continuous member from zones which are stressed plastically to zones which are not yet plastic. Having sufficient ductility helps to satisfy the lower bound theorem of plasticity in design, which in turn ensures that no undesired collapse mechanism occurs prior to the expected failure mode. In addition, the ability for redistribution of BM in conventional statically indeterminate RC members allows for an efficient and economical design by reducing the cross-sectional area or internal reinforcement in the zones with maximum BM and congested reinforcement (Mattock, 1958; Scott and Whittle, 2005).

If a structure is not ductile or if the original ductility is fully lost after strengthening, no advantage can be taken of moment redistribution (MR) in the structure. However, what level of ductility is required to allow some MR to occur? A lack of sufficient research looking at a link between the precise reduction in the ductility of RC members after FRP strengthening and any possible MR thereafter has resulted in uncertainty in this issue such that design standards worldwide have ignored (or overly conservatively limited) the exploitation of MR in FRP-strengthened RC flexural members (e.g. ACI-440-2R, 2008; TR55, 2012). This means that RC members which need to be strengthened using FRP must be designed based on assumed elastic flexural behaviour up to failure, despite the fact that the original structure may have been designed with full consideration of ductility and MR. As Ibell and Silva (2004) described, this results in a very complex design condition because, after strengthening, the zones which were originally designed for a reduced BM must now be designed according to the original un-redistributed elastic BM plus any additional BM which is required for the strengthening requirement. Therefore, it can result in the need for great quantities of strengthening material. Consequently, it is very important that the profession knows exactly the level of MR which is likely, lest vast quantities of materials are wasted unnecessarily.

Quantifying MR in FRP-strengthened RC beams is potentially a complex problem. A few theoretical research studies have been conducted on this issue. Oehlers *et al.* (2004) claimed that it is very hard to determine the adequacy of ductility in an FRP-strengthened RC beam. They proposed two different analytical approaches, called the ‘Flexural rigidity approach’ and the ‘Plastic hinge approach’, for quantifying MR. In the first approach, stiffness variation is accommodated within zones with sagging and hogging BMs, while in the second approach it is assumed that flexural stiffness is constant along the entire beam except for the zones where plastic hinges are formed. They discuss that the hinge approach cannot be applied to FRP-strengthened beams as, usually, FRP debonding typically occurs prior to concrete crushing, and the strengthened region usually behaves elastically prior to debonding. This means that no plastic hinge (i.e. a region of constant BM capacity with increase in curvature) can be formed in FRP-strengthened zones. However, using the rigidity approach, they indicate that ductility of FRP-plated beams is lower than that of steel-plated beams. A simplified theoretical method was proposed by Ashour *et al.* (2004) to predict the load capacity of an FRP-strengthened beam. The method relies on equilibrium of forces and compatibility of deformations. This method can be used to calculate MR at failure, although it is assumed that the critical sections in the sagging and hogging zones reach their moment capacity at the time of failure.

Silva and Ibell (2008) applied a theoretical strategy to investigate ductility in such structures. They showed that an RC beam can still exhibit rotation capacity even after FRP strengthening, provided that the strengthened section has sufficient curvature ductility. They demonstrated that although ductility is reduced in general, BM can be redistributed out of an FRP-strengthened section by at least 7.5%, if the section has a curvature ductility capacity (defined as the ratio of the curvature at ultimate failure to the curvature at steel first yield) of at least 2.0, and a certain minimum strain is obtained in the steel reinforcement. This finding is based on an assumption that failure occurs through debonding of the FRP at a typical strain of 0.8%. This method appears to be somewhat complex to implement in a general sense. A few studies (Dalfré and Barros, 2011; Breveglieri *et al*., 2012) have also been conducted recently to predict or analyse MR in strengthened structures using an FEM-based computer program. The results showed that the technique and configuration of strengthening significantly influences the degree of MR. Santos *et al*. (2013) and Lou *et al*. (2015) presented finite element models to predict MR in FRP-reinforced RC beams. The models basically assume a specific damage model for concrete, elastic-plastic behaviour for steel, isotropic behaviour for the steel-concrete interface, linear elastic behaviour for FRP and perfect bond for the FRP-concrete interface. The numerical simulations showed good comparison with the experimental findings.

There is a lack of sufficient research on defining clearly and relatively simply the extent to which MR can be relied on when an RC beam is strengthened using FRP. This paper presents a new numerical model which allows redistribution of BM in an FRP-strengthened RC beam to be quantified rigorously. To predict the flexural behaviour of the strengthened beam, the model applies a fundamental approach which is based on structural mechanics, not on empirical limits, and allows stiffness variations along the length of the beam to be found and updated during loading, using an iterative approach. The degree of MR can be determined at any point along the beam length, and at any applied load until failure. The new model is verified against experimental findings which exist in the literature. It must be noted that this paper only aims to present a model which can predict how MR occurs over the loading cycle, up to failure, based on assumed values for FRP debonding or rupture, and not to predict the actual failure mode. However, if required or desired, models for predicting failure modes (including concrete crushing, FRP debonding/rupture, and even shear failure) can be accommodated in the numerical model presented here.

2. MOMENT REDISTRIBUTION

In this section, the implication of MR is briefly presented through a particular (simple) example. An idealised elastic-plastic relationship between curvature (K) and bending moment (M) is considered in Figure 1 for all sections throughout the beam shown in Figure 2. A section reaches its moment capacity of M_u at a curvature of φ_y when the steel reinforcement yields, and the section fails at an ultimate curvature of φ_u.

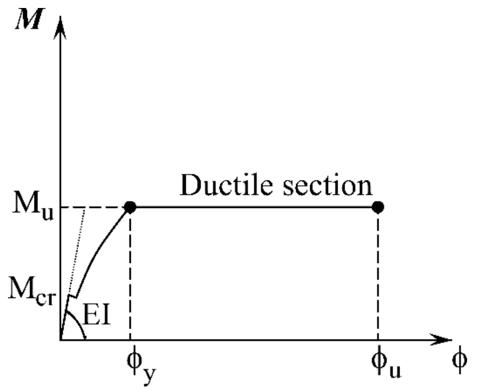

Figure 1: A theoretical elastic-plastic M-K relationship adopted for the example beam

Shown in Figure 2 is a statically-indeterminate two-span conventional RC beam which is loaded symmetrically under a concentrated load at each mid-span. A constant flexural stiffness of *EI* is assumed along the entire length of the beam before loading.

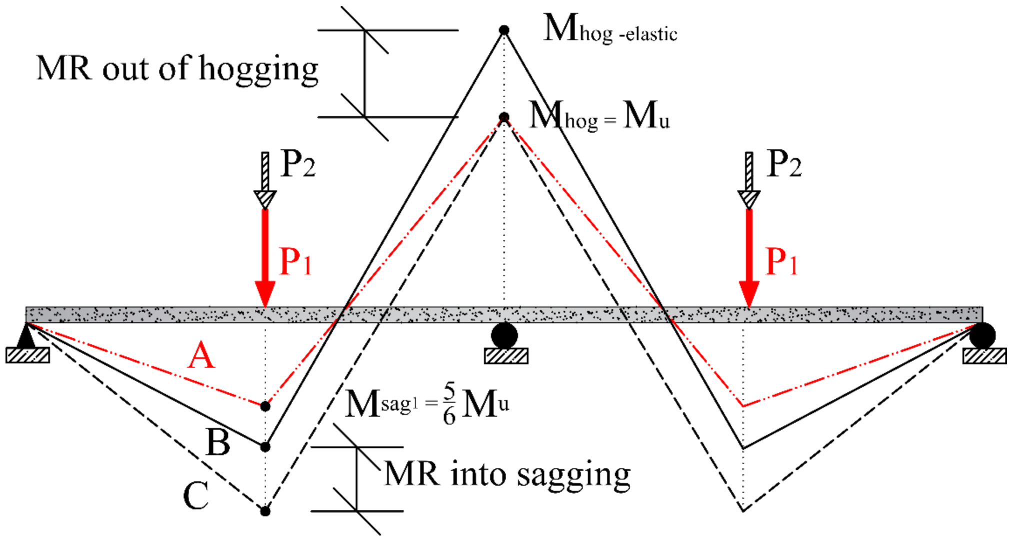

Figure 2: A simple two-span RC beam and the implication of MR

Within the elastic range across the entire beam, the ratio of the hogging-zone BM to the sagging-zone BM remains constant. According to 'elastic theory', this ratio is 1.20 for this particular example. As long as this ratio is fixed, no redistribution of BM occurs in the beam. If the load increases further (Load P1, as shown in Figure 2), the steel reinforcement will yield first in the hogging zone (over the central support), due to the loading arrangement adopted, and this zone will just reach its moment capacity of M_u, at which point the sagging-zone BM is $\frac{5}{6} M_u$ (line A in Figure 2). Any further loading will cause only the sagging-zone BM to increase as the hogging-zone BM must remain constant at M_u. As shown in Figure 2 by a black dashed line (line C), ultimate failure occurs when the sagging zone at mid-span also reaches its moment capacity of M_u (at Load P1+P2). The black solid line (line B) shows the theoretical elastic BM diagram at the failure load, assuming that there had been no stiffness variation during loading to have led to MR. The primary reason which allows the increase in BM in the sagging zone (from $\frac{5}{6}\,M_u$ to M_u) to occur is the presence of curvature ductility of the hogging zone. It is seen that the ratio of hogging-zone BM to sagging-zone BM becomes 1.0 at ultimate failure, rather than the elastic ratio of 1.20. Hence, it can be concluded that BM has been redistributed from the hogging zone to the sagging zone, as shown in Figure 2.

But this process becomes more complicated when FRP is added. As shown in Figure 3, there are various zones in an FRP-strengthened RC member which can be unstrengthened (such as Zone A), or lightly strengthened (such as Zone B), or heavily strengthened (such as Zone C). When the member is loaded, these zones experience different rates of stiffness variation.

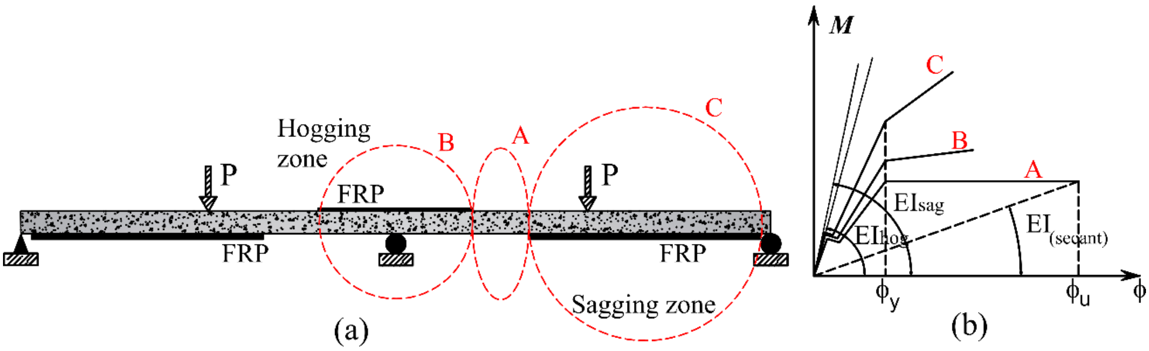

Figure 3: (a) Schematic image of a continuous FRP-strengthened beam; and (b) M-K relationships for different zones of the beam

As illustrated in Figure 3, there is no horizontal plastic plateau in the M-K relationship of the FRP-strengthened zones. This means that no plastic hinge is formed in the strengthened zones even if the steel reinforcement yields as the FRP withstands the applied load elastically until failure. In addition, various amounts of FRP can be added to the member in various configurations, affecting the mode of failure and flexural behaviour of the strengthened member. These complexities indicate a need for a fundamental solution to this problem. A novel numerical model is described in the following section which can predict the flexural behaviour of FRP-strengthened RC members using a fundamental approach. The model relies only on structural mechanics and tracks stiffness variations in the beam logically, whether strengthened or not.

3. THE NUMERICAL MODEL

The new model employs sectional analysis to determine stiffness variations in the beam over the loading cycle. A computer programme has been written for the numerical calculations and analytical modelling. The given beam is initially subdivided into a large number of narrow vertical segments (e.g. slices of 10mm thickness). The full M-K relationship is found for each section along the length of the beam, whether strengthened with FRP or not. It is obvious that the more precise the relationship found between moment and curvature, the more accurate the prediction made for the flexural behaviour of the beam.

3.1 Determination of the M-K relationship

To find a precise relationship between Moment and Curvature for each section, required data for the numerical model include the geometry, specifications of the internal reinforcement and strengthening materials, and constitutive material models.

Figure 4 illustrates the material models adopted for concrete, steel and FRP in this numerical technique. A parabolic curve has been adopted for the stress-strain relationship of the concrete in compression, according to

BS EN 1992-1-1: 2004 (Figure 4(a)). ε_{c1} is the strain at peak stress, and is equal to (ε_{c1} =) $0.7\times f_{cm}^{0.31}$, where f_{cm} is the mean compressive strength of concrete at 28 days. ε_{cu1} is the ultimate compressive strain in concrete which is considered to be 0.35% in this parabolic model. A linear relationship between stress and strain has been adopted for concrete in tension, according to BS EN 1992-1-1: 2004 (Figure 4(b)). The tensile strength (f_{ctm}) is equal to $0.3\times f_{ck}^{(2/3)}$ (in MPa), where f_{ck} is the characteristic cylinder strength of concrete ($f_{ck} = f_{cm}$ -8 (MPa)). In addition, $\varepsilon_{ct} = f_{ctm}/E_{cm}$, where ε_{ct} is the tensile strain, and E_{cm} is the modulus of elasticity of concrete (GPa), and is equal to $22 \times [(f_{cm})/10]^{0.3}$. Softening of the concrete under tension is ignored in the numerical model as it does not play any role in the degree of MR quantified at failure. The behaviour of steel reinforcement is represented by a bilinear model (Figure 4(c)) with a linear elastic branch ending at the yield stress (f_y), and a linear inclined plastic branch which shows strain hardening in the steel reinforcement after yielding, ending at ultimate fracture (f_u). The relationship between stress and strain for FRP is considered linear-elastic up to rupture (Figure 4(d)).

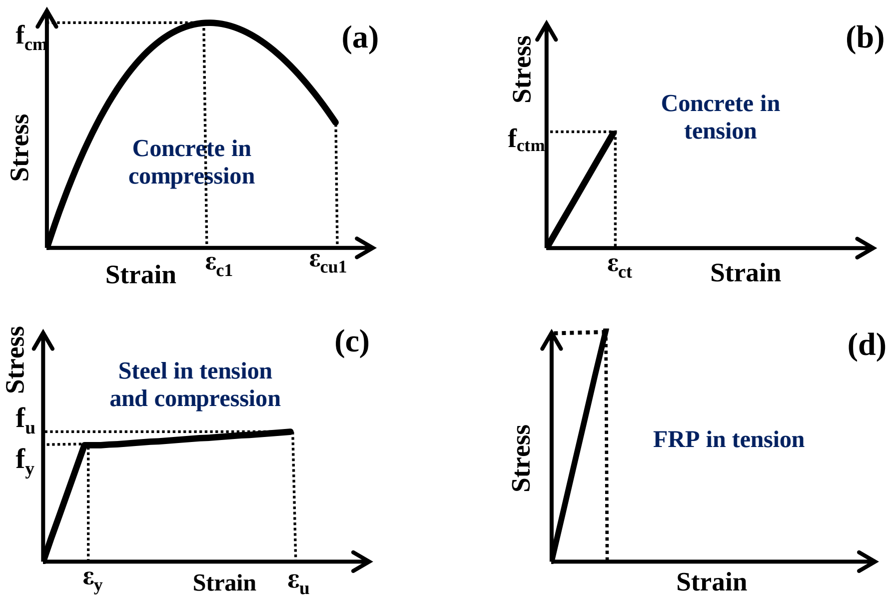

Figure 4: Constitutive material models adopted for the numerical model

The M-K relationship for each section along the beam is found according to standard procedures, which are outlined here for completeness. Each cross-section along the beam is divided into horizontal segments of 1mm thickness. For varying curvatures starting from zero, strains in each segment are found using an initial estimate for the neutral axis depth (k_d), by assuming that there is a perfect bond between concrete and steel reinforcement, and between concrete and FRP, and also that plane sections remain plane. Using the adopted material models, the stresses and forces are calculated separately for the tension and compression zones of the section, by knowing the corresponding strains in each constitutive material. As shown in Figure 5, the overall tension force (T) includes tension in the steel reinforcement (T_s), concrete (T_c) and FRP (T_f), and the overall compression force (C) includes compression in the concrete (C_c) and compression steel (C_s). If the overall tension force is not in equilibrium with the overall compression force (i.e. $T \neq C$), the neutral axis position is adjusted and the forces are recalculated while maintaining the same curvature. This calculation is performed iteratively until equilibrium is achieved and a precise position for the neutral axis is found. Note that it is a simple matter to assume $T_c=0$ if this is thought sensible.

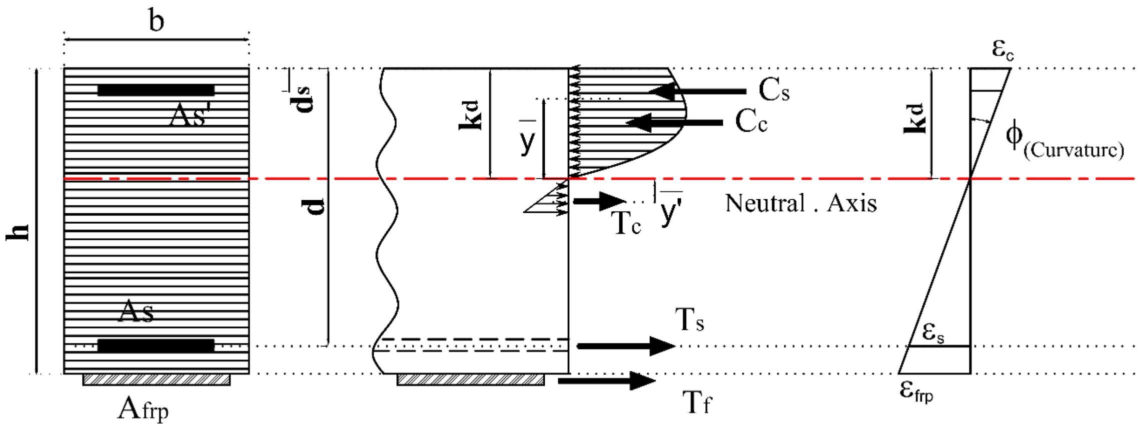

Figure 5: Calculation of tension and compression forces in an FRP-strengthened RC section

Finally, the corresponding moment of resistance (M) is determined from the calculated k_d for the adopted level of curvature by taking moments for the tension and compression forces about the neutral axis:

$$\boldsymbol{M} = (\boldsymbol{C_c} \times \bar{y}) + \big(\boldsymbol{C_s} \times (\boldsymbol{k_d} - \boldsymbol{d_s})\big) + (\boldsymbol{T_c} \times \bar{y}') + \big(\boldsymbol{T_s} \times (\boldsymbol{d} - \boldsymbol{k_d})\big) + (\boldsymbol{T_f} \times (\boldsymbol{h} - \boldsymbol{k_d})) \qquad \textit{Eq. 1}$$

where $\bar{y}$ represents the distance between the neutral axis and the centroid of the concrete's compression zone, and is found from Eq. 2.

$$\bar{y} = (\boldsymbol{\Sigma}(\boldsymbol{A_i} \times \boldsymbol{C_{c_i}} \times \boldsymbol{y_i})/\boldsymbol{\Sigma}(\boldsymbol{A_i} \times \boldsymbol{C_{c_i}})) \qquad \textit{Eq. 2}$$

where A_i is the area of horizontal layer i, C_{ci} is the compression force in layer i, and y_i is the depth from the centroid of layer i to the neutral axis. Similarly, $\bar{y}'$ is the distance between the neutral axis and the centroid of the concrete's tension zone. A complete M-K relationship is found for all cross-sections along the beam by repeating these calculations for different curvature values, until failure. Ultimate failure is simply controlled through specifying limiting values for strains in the concrete and FRP. In this study, a typical strain value of 0.35% is adopted for crushing of concrete in compression, and values of 0.8% and 1.5% are assumed for failure of the FRP through debonding (usual) and rupture (if the FRP is fully anchored) respectively. These values are based on what has been observed in the literature but are not definitive. If required, these assumed values can be refined appropriately.

3.2 Determination of the real BM distribution

Now, the real distribution of BM along the beam length is determined for each applied load using the M-K relationships found in the previous section. For a load increment starting from zero, the elastic BM is determined for all sections along the beam using, for example, the virtual work method and using the baseline uncracked flexural stiffness for each section. Knowing the BM at each section and using the corresponding M-K relationship, the curvature of each section is found. From 'elasticity theory', the actual effective stiffness, $(EI)_{\text{effective}}$, can then be found for each section according to:

$$(\boldsymbol{EI})_{\boldsymbol{effective}} = \frac{\boldsymbol{M}}{\boldsymbol{K}} \qquad \textit{Eq. 3}$$

where M is the bending moment and K is the curvature of each section. Now, a new distribution of bending moments is found along the beam, knowing the new stiffness of all sections. As shown schematically in Figure 6, this set of calculations is performed iteratively until it converges and a distribution of BM is found in the beam at the particular load increment. Convergence is defined by comparing the new BM diagram with the previous diagram after each iteration, and the iterative calculations are stopped when the difference between the two diagrams is less than 1N.mm at the point of maximum BM along the beam.

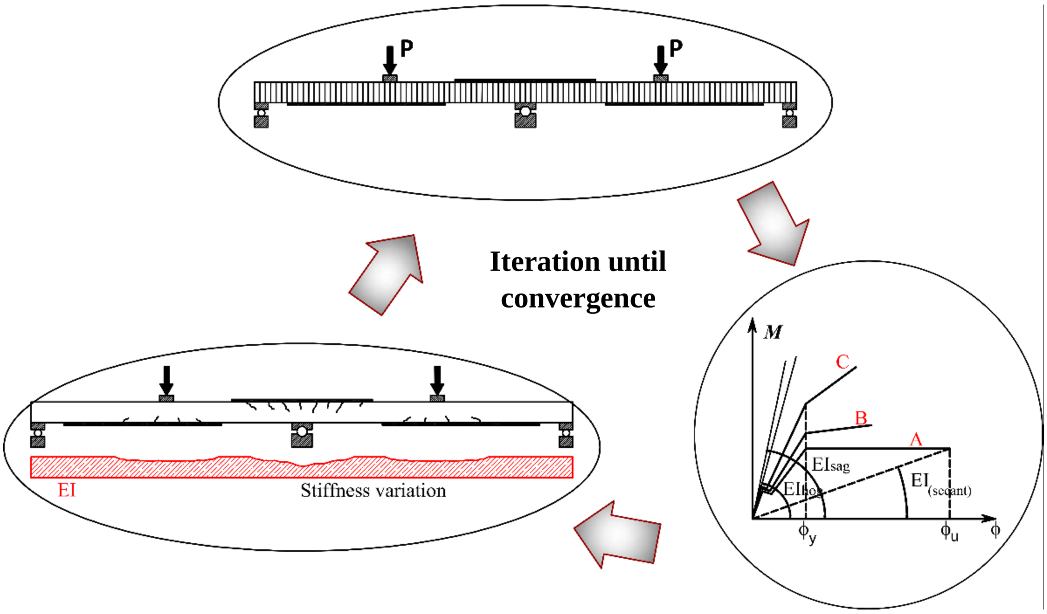

Figure 6: A schematic image of how iterations are conducted using the new numerical model

3.3 Moment redistribution quantification

The degree of MR is calculated at each load increment using the following equation, as described by Cohn (1986), Cohn and Lounis (1991) and Rebentrost *et al.* (1999):

$$\boldsymbol{MR}\ (\%) = \mathbf{100} \times \left(\mathbf{1} - \frac{\boldsymbol{M_{redis}}}{\boldsymbol{M_{elas}}}\right) \qquad \textit{Eq. 4}$$

where $\boldsymbol{M_{redis}}$ is the last BM at a critical location obtained from the iterative approach, taking into account variation of stiffness, and $\boldsymbol{M_{elas}}$ is the theoretical elastic BM determined from elastic analysis at the same location, assuming an initial uncracked elastic flexural stiffness. These calculations are repeated for each load increment, and MR can be quantified, until a critical section reaches one of the limiting strains described previously, and the section fails through failure of the concrete or FRP. It is to be noted that shear failure is assumed to be prevented through providing sufficient shear reinforcement along the beam, and that shear deformations are negligible.

4. ADVANTAGES OF THE NEW MODEL

The new model allows MR to be assessed and quantified simply for design purposes, using structural mechanics in a logical way, without any need to rely on empirical or complex equations for the calculation of rotation capacity or curvature ductility in an FRP-strengthened RC beam. In addition, the following advantages can be identified:

- Redistribution of BM can be quantified at any stage of loading, from the beginning right through to failure.
- Various changes and features of the structural behaviour of the beam can be monitored, including crack initiation, steel yield, FRP debonding, FRP rupture, and concrete crushing. All are controlled via the M-K relationship of the sections without the need for any explicit assumption about the ‘plastic’ behaviour of the strengthened beam.
- The position of any critical point is easily identified. Also, the degree of MR can be quantified at any point along the length of the beam, at any load.
- The model is compatible with any material model for the constitutive materials, and for any assumed failure strain limits.

- Any beam shape or dimensions, loading arrangements, and techniques of FRP strengthening can be accommodated by the new model, even if asymmetric and/or multi-span.

It should be noted that the proposed model shows less accurate results when the zone which is controlling MR is unstrengthened. This is because, in this specific case, the plastic plateau of the M-K relationship related to the critical zone is almost a horizontal line (line **A** in Figure 3(b)), making it difficult or impossible to define a unique and accurate curvature for a given BM after steel yield. Hence, the numerical model requires a non-horizontal plastic plateau to be able to complete the computational iteration required for the calculation of BMs described earlier. To overcome this problem, an alternative approach based on equilibrium of BMs in the sagging and hogging zones was developed (Tajaddini, 2015). This is not required for the cases presented in this paper.

5. VERIFICATION OF THE NEW MODEL

In this section, the numerical model is validated against existing experimental data in the literature. Figure 7 illustrates a schematic image of the geometry and loading arrangement of the experiments conducted by El-Refaie *et al.* (2003), Oehlers *et al.* (2004), and Aiello *et al.* (2007). All specimens were two-span rectangular RC beams which were loaded under concentrated loads at each mid-span, symmetrically. The experiments were carried out to investigate MR arising after flexural strengthening of continuous RC flexural members. Various strengthening techniques were used for the specimens in the different test series. Details of the test specimens, specifications of the test layouts, and configurations of FRP strengthening are summarised in Table 1.

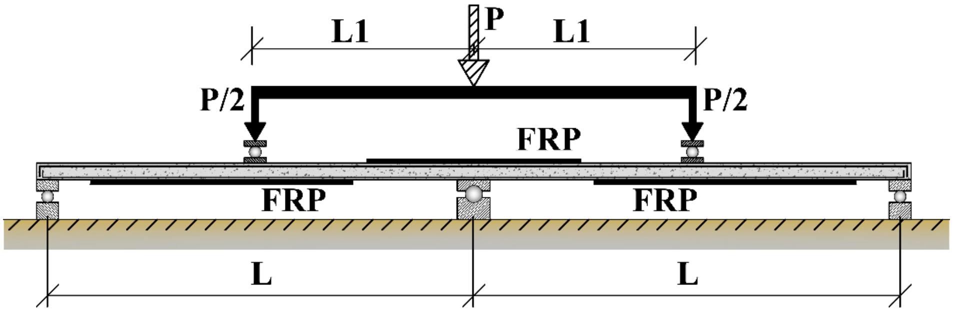

Figure 7: A schematic image of the existing experimental work in the literature

Table 1: Details of some existing experiments in the literature

Beam	Width*Depth (mm)	L (mm)	L1 (mm)	Top steel bars	Bottom steel bars	FRP position	FRP EA value (kN)	Steel yield strength (MPa)	Concrete strength (MPa)
H2[*]	150*250	3830	1915	2T8	2T20	Hogging	6180	505-510	43.5[cu]
H3[*]	150*250	3830	1915	2T8	2T20	Hogging	18500	505-510	33.0[cu]
H4[*]	150*250	3830	1915	2T8	2T20	Hogging	30900	505-510	33.2[cu]
H5[*]	150*250	3830	1915	2T8	2T20	Hogging	18500	505-510	46.0[cu]
H6[*]	150*250	3830	1915	2T8	2T20	Hog&Sag	6180[#]	505-510	44.0[cu]
SF2[**]	375*120	2400	1200	2T12	4T16	Hogging	8640	601-540	39.0[cy]
SF3[**]	375*120	2400	1200	2T12	4T16	Hogging	13800	601-540	39.0[cy]
SF4[**]	375*120	2400	1200	2T12	4T16	Hogging	10500	601-540	48.0[cy]
S_{0-1}[***]	150*200	1750	800	2T12	2T12	Hogging	5700	557	21.1[cy]
S_{1-1}[***]	150*200	1750	800	2T12	2T12	Hog&Sag	5700[#]	557	21.1[cy]

[*]Beams tested by El-Refaie *et al.* (2003); [**]Beams tested by Oehlers *et al.* (2004); [***] Beams tested by Aiello *et al.* (2007).
[#]EA value at each of the sagging and hogging zones; [cu] Cube strength; [cy] Cylinder strength.

Figure 8 compares the experimental data and the numerical results obtained from the new model for the failure load and hogging-zone BM at failure in the specimens. It should be noted that the numerical results were obtained assuming similar failure strains for the FRP debonding or rupture to those recorded experimentally. Except for Beam SF4, a reasonable agreement can be seen between the experimental and numerical results, indicating the ability of the numerical model to predict the flexural behaviour of continuous RC members strengthened using FRP.

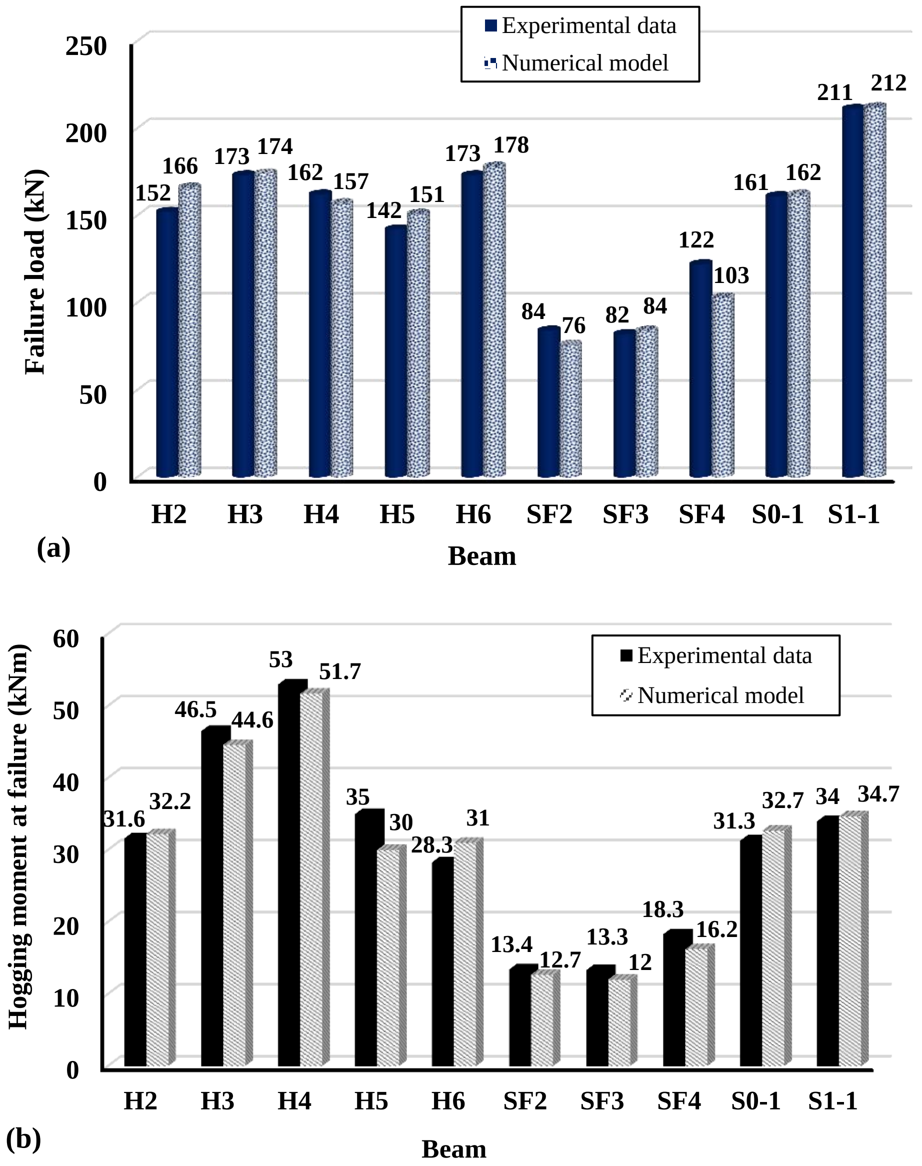

Figure 8: Comparison of the experimental data with the numerical model. (a) Failure load; (b) Hogging moment at failure

It is observed that the numerical model generally predicts correctly the flexural softening and mode of failure in the critical zones of the tests reported in the literature. Using the proposed model, progression in flexural softening can be tracked and monitored logically. Table 2 provides a comparison between the experimental data and corresponding numerical results. Summarised in the table are the modes of failure, the load values at which first cracking occurred, the load values at which first steel yield occurred, and the values of experimentally recorded strain in the FRP at failure. All the numerical predictions are based on the recorded strains. As seen in Table 2, the correlation between the experimental and numerical data, over the full extent of loading, is reasonably good.

Table 2: Experimental data versus numerical predictions over the loading cycle

Beam	Failure mode (Exp.)	Failure mode (Numerical)	Exp. cracking load (kN)	Numerical cracking load (kN)	Exp. yield load (kN)	Numerical yield load (kN)	FRP Failure strain (exp.)
H2	FRP rupture	FRP rupture	19.5	20.1	118	102	1.6%
H3	FRP debonding	FRP debonding	20	20.3	142	131	0.8%
H4	FRP debonding	FRP debonding	20.5	21	155	140	0.62%
H5	FRP debonding	FRP debonding	20	20.2	140	128	0.4%
H6	FRP rupture	FRP rupture	19.5	19.8	121	106	1.6%
SF2	FRP debonding	FRP debonding	20.1	21.5	-	96	0.29%
SF3	FRP debonding	FRP debonding	33.6	34	-	122	0.25%
SF4	FRP debonding	FRP debonding	36.7	34.8	-	104	0.42%
S_{0-1}	CC*, followed by FRP rupture	CC*, followed by FRP rupture	22.7	19.8	146	132	1.5%
S_{1-1}	CC*, followed by FRP rupture	CC*, followed by FRP rupture	21.2	19.1	129	117	1.5%

*CC = Concrete Crushing.

MR was quantified for the beams tested, using the numerical model and applying Eq. 4, and then compared with the experimental data reported in the corresponding literature. A reasonable correlation is observed between the experimental and numerical results at failure, as illustrated in Figure 9, indicating that the new model can reasonably predict the degree of MR in continuous FRP-strengthened RC beams. In addition, as seen in Figure 9 and reported in the corresponding literature, MR can occur in FRP-strengthened RC beams to a reasonable extent, even up to 35% in the present study, although increasing the amount of FRP in the zone from which BM is redistributed reduces the level of redistribution, as observed in Beam H4. Also, this may cause BM to be redistributed conversely from the sagging zone to the hogging zone, as observed in Beam S_{0-1}. It should be noted that a prediction for MR, assuming a strain of 0.8% (where the FRP debonded in the test) and 1.5% (where the FRP actually ruptured in the test), has also been provided in Figure 9, such that predicted results are consistent. Generally, such predictions are adequate across the full range.

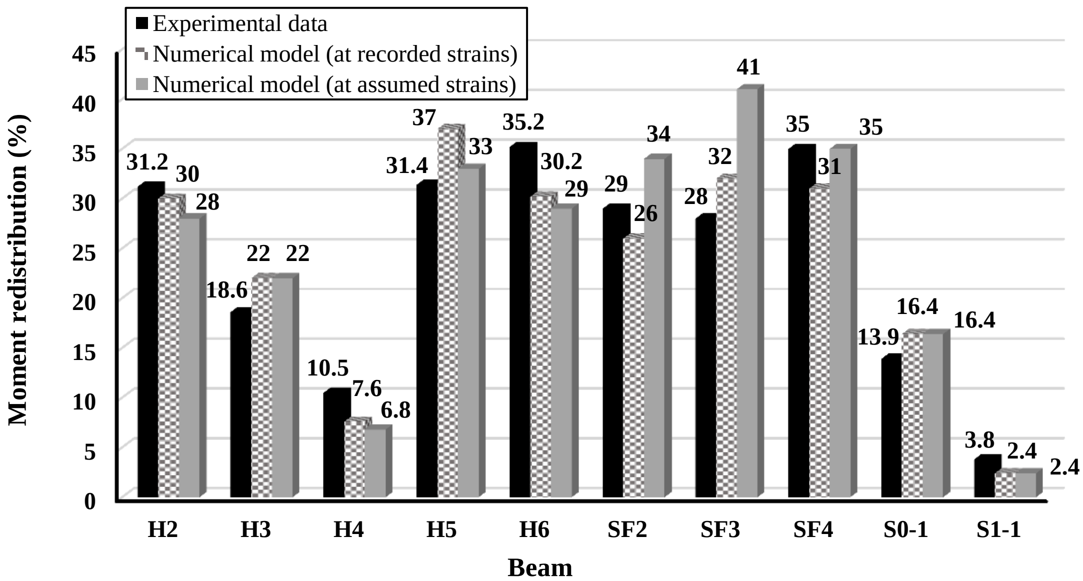

Figure 9: Comparison of the experimental MR data with those predicted numerically

It is worth noting that, as seen in Figure 9, the initial condition and design of the specimens influence their capacity for MR such that beams S_{0-1} and S_{1-1} exhibited a lower degree of MR at failure compared to the others. This is due to the fact that the arrangement of internal reinforcement in beams S_{0-1} and S_{1-1} reduces their overall capacity for MR, while the other beams have higher capacities due to the difference between the proportion of steel reinforcement in the top and bottom of the cross section. It should also be noted that the reason for beam H4 exhibiting low capacity for MR is the quantity of the FRP used for strengthening.

6. Conclusions

A new numerical approach has been proposed in this paper to model the flexural behaviour of RC continuous members strengthened using FRP materials. The model applies basic structural mechanics, and can quantify redistribution of BM over the full loading cycle. The numerical model has been validated against existing experimental data in the literature. The following conclusions are drawn based upon the study conducted:

- Various beam geometries, loading arrangements, strengthening techniques or configurations can be adopted to the numerical model.
- A good comparison has been observed between the numerical results obtained from the model and the test findings and observations in terms of predicting the flexural behaviour of continuous FRP-strengthened RC members over loading, also in terms of failure mode, failure load and BM at failure.
- A reasonable agreement has been seen between the numerical predictions and experimental results for the degree of MR which occurred in the test specimens, assuming that the debonding strain in the FRP remained constant. However, the failure mode could potentially be predicted in future work by adopting a reliable debonding/failure model.
- This work opens the possibility for MR to be quantified and included explicitly in FRP-strengthening design guidelines.

Acknowledgement

The authors gratefully acknowledge the research funding provided by the Engineering and Physical Sciences Research Council (EPSRC: EP/K019015/1) and the project partners (Concrete Repairs Ltd, Fyfe, Highways England, WSP/Parsons Brinckerhoff and Tony Gee and partners) for this research project. This study was a re-analysis of existing data that are publicly available. Further documentation about data processing are available from the University of Bath data archive at http://doi.org/10.15125/BATH-00178.

List of notations

A_{frp} Area of the FRP

A_s Area of the tension steel reinforcement

A_{sc} Area of the compression steel reinforcement

C Total force in compression

C_c Compression in the concrete

C_s Compression in the steel reinforcement

d Effective depth to the tension reinforcement

d_s Effective depth to the compression reinforcement

E_{cm} Young's modulus of concrete

E_f Tensile modulus of the FRP

EA Tension stiffness of the FRP

EI Flexural stiffness

f'_c Compressive strength of concrete

f_y Yield strength of steel reinforcement

f_{ck} Characteristic cylinder strength of concrete

f_{ctm} Characteristic tensile strength of concrete

f_{cm}	The mean compressive strength of concrete at 28 days
h	Overall height of beam
K_d	Neutral axis depth
M	Bending moment
M_{elas}	Theoretical bending moment determined from elastic analysis
M_{redis}	Redistributed bending moment
M_u	Moment capacity
MR	Moment redistribution
P	Applied load
P_u	Ultimate (failure) load
T	Total force in tension
T_c	Tension in the concrete
T_f	Tension in the FRP
T_s	Tension in the steel reinforcement
$\bar{y}$	Depth from neutral axis to the centroid of the concrete's compression zone
$\bar{y}'$	Depth from neutral axis to the centroid of the concrete's tension zone
ε	Strain
ε_{c1}	Concrete strain at peak stress
ε_{cu1}	Ultimate strain in the concrete
ε_f	Strain in the FRP
ε_s	*S*train in the tension steel reinforcement
ε_{ct}	Tensile strain in the concrete
σ	Stress
φ_u	Ultimate curvature
φ_y	curvature at steel yield

References

ACI 440.2R: 2008, Guide for the Design and Construction of Externally Bonded FRP Systems for Strengthening Concrete Structures. ACI.

Aiello, M. A., & Ombres, L., 2007. Moment redistribution in continuous reinforced concrete beams strengthened with carbon-fibre-reinforced polymer laminates. *Mechanics of composite materials*, *43*(5), pp. 453-466.

Ashour, A. F., El-Refaie, S. A., & Garrity, S. W., 2004. Flexural strengthening of RC continuous beams using CFRP laminates. *Cement and concrete composites*. *26*(7), pp. 765-775.

Beeby, A. W., 1997. Ductility in reinforced concrete: why is it needed and how is it achieved?. *Structural Engineer*, *75*(18), pp. 311-318.

Breveglieri, M., Barros, J. A., Dalfré, G. M., & Aprile, A., 2012. A parametric study on the effectiveness of the NSM technique for the flexural strengthening of continuous RC slabs. *Composites Part B: Engineering*, 43(4), 1970-1987.

BS EN 1992-1-1: 2004, *Eurocode 2: Design of concrete structures*. General rules and rules for buildings. BSI.

Casadei, P., Nanni, A., Galati, N., Ibell, T., and Denton, S., 2003. Moment redistribution in continuous CFRP strengthened concrete members: experimental results. *International Conference Composites in Construction - CCC2003*. Cosenza, Italy, 307-312, September 16-19.

Cohn, M.Z. and Lounis, Z., 1991. Moment redistribution in structural concrete codes. *Canadian Journal of Civil Engineering*, 18(1), pp.97-108.

Cohn, M.Z., 1986. Continuity in prestressed concrete. In *Partial prestressing, from theory to practice* (pp. 189-256). Springer Netherlands.

Concrete Society Technical Report 55, 2012. *Design guidance for strengthening concrete structures using fibre composite materials*. The Concrete Society, UK.

Dalfré, G., & Barros, J., 2011. Flexural strengthening of RC continuous slab strips using NSM CFRP laminates. *Advances in Structural Engineering*, 14(6), 1223-1245.

El-Refaie, S. A., Ashour, A. F., & Garrity, S. W., 2003. Sagging and hogging strengthening of continuous reinforced concrete beams using carbon fibre-reinforced polymer sheets. *ACI structural journal*. *100*(4), pp. 446-453.

Holloway, L. C., & Leeming, M. B., 1999. Strengthening of reinforced concrete structures. *Woodhead Publishing Ltd and CRC Press*.

Ibell, T. J., & Silva, P. F., 2004. A theoretical strategy for moment redistribution in continuous FRP-strengthened concrete structures. In *Proceedings of conference ACIC-2004*. The University of Surrey, Guildford, UK. 20-22 April. pp. 144-151.

Lou, T., Lopes, S. M., & Lopes, A. V., 2015. Neutral axis depth and moment redistribution in FRP and steel reinforced concrete continuous beams. *Composites Part B: Engineering*, 70, 44-52.

Mattock, A. H., 1959. Redistribution of design bending moments in reinforced concrete continuous beams. In *ICE Proceedings*, 13(1), pp. 35-46. Thomas Telford.

Ohlers, D.J., Ju, G., Liu, I.S.T. and Seracino, R., 2007. A generic design approach for EB and NSM longitudinally plated RC beams. *Construction and Building Materials*. 21, 697–708.

Oehlers, D., & Seracino, R., 2004. *Design of FRP and steel plated RC structures: retrofitting beams and slabs for strength, stiffness and ductility*. Elsevier.

Oehlers, D. J., Ju, G., Liu, I. S. T., & Seracino, R., 2004. Moment redistribution in continuous plated RC flexural members. Part 1: neutral axis depth approach and tests. *Engineering structures*. *26*(14), pp. 2197-2207.

Rebentrost, M., Wong, K.W. and Warner, R.F., 1999. Moment redistribution and rotation capacity in prestressed concrete structures. *Mechanics of Structures and Materials*, p. 97-102.

Santos, P., Laranja, G., França, P. M., & Correia, J. R., 2013. Ductility and moment redistribution capacity of multi-span T-section concrete beams reinforced with GFRP bars. *Construction and Building Materials*, *49*, pp. 949-961.

Scott, R. H., & Whittle, R. T., 2005. Moment redistribution effects in beams. *Magazine of concrete research*. *57*(1), 9-20.

Silva, P. F., & Ibell, T. J., 2008. Evaluation of moment distribution in continuous fibre-reinforced polymer-strengthened concrete beams. *ACI Structural Journal*. *105*(6), pp. 729-739.

Tajaddini, A., 2015. Investigation of moment redistribution in FRP-strengthened slabs and T-beams. Ph.D. thesis. University of Bath, UK.

Teng, J. G., Chen, J. F., Smith, S. T., & Lam, L., 2001. *FRP: strengthened RC structures*. Wiley, New York.

List of figures:

List of tables: